2nd International Conference on Engineering Optimization
September 6 - 9, 2010, Lisbon, Portugal

Aerodynamic shape optimization using adaptive remeshing

Mohammad Kouhi[1], Gabriel Bugeda[1], DongSeop Lee[1] and Eugenio Oñate[1]
[1]International Center for Numerical Methods in Engineering
(CIMNE/UPC)

Abstract:
Adaptive mesh refinement is one of the most important tools in Computational Fluid Dynamics (CFD) for solving complex engineering design problems. The paper investigates two practical transonic aerofoil design optimization problems using a genetic algorithm coupled with an Euler aerodynamic analysis tool. The first problem consists in the minimization of transonic drag whereas the second is a reconstruction transonic problem solved by minimizing the pressure error. In both cases, the solutions obtained with and without adaptive mesh refinement are compared. Numerical results obtained by both drag minimization and reconstruction design clearly show that the use of adaptive mesh refinement reduces the computational cost and also produces a better solution.

Keywords: Adaptive mesh, Euler equation, Reconstruction design, Drag minimization, Genetic algorithm.

1. Introduction

Adaptive mesh refinement is one of the most important tools in the Computational Fluid Dynamics (CFD) and advanced engineering design. CFD technologies have improved a lot and can solve real live problems. However, the reduction of computational cost and solution accuracy improvement still remain as important challenges [1-5]. The paper introduces adaptive mesh refinement coupled with CFD in the context of optimum shape design as an alternative method due to its advantages: low computational cost and result accuracy.

When using adaptive mesh refinement methodologies, a minimum level of error is obtained by paying a reasonable amount of computational cost using the smallest number of degrees of freedom. Two main components of adaptive refinement method are a reliable error estimator/indicator and a mesh refinement strategy; once the CFD calculates the flow characteristics of each element, a reliable error indicator determines where the discretization error is more or less than predefined values. This is the concept of error estimation in the Finite Element Method (FEM) that evaluates the level of error as a function of flow variables, element size and also interpolation order. Even though the most conventional approach during optimization is to use a fixed uniform fine mesh, this paper uses an adaptive remeshing technique for the analysis of every individual to guarantee the production of accurate results during the optimum design process.

In this paper, two practical transonic aerofoil design problems using adaptive mesh techniques coupled to Genetic Algorithms (GAs) [6-8] and Euler flow analyzer [9] are addressed. The first test considers drag minimization subject to thickness constraint with and without adaptive remeshing technique. Reconstruction of transonic airfoil design with and without adaptive remeshing technique is considered for the second test. These design problems under transonic speeds need to be solved with a fine mesh, particularly near the object, to capture the shock waves that will cost high computational time and require solution accuracy. The first design case attempts to find a transonic airfoil shape which can produce lower drag when compared to the baseline design [10, 11]. The second design case tries to capture the same pressure distribution as the baseline design [12, 13]. The numerical results obtained with both optimization problems show the obtainment of direct benefits in the reduction of the total computational cost through a better convergence to the final solution, and the improvement of the solution quality when an adaptive remeshing technique is coupled with the optimum design strategy. The paper will show how to reduce computational cost and how to improve solution accuracy using adaptive remeshing techniques for solving transonic aerofoil design optimization.

The rest of paper is organized as follows; Section 2 describes the optimization Method; Genetic Algorithm. Section 3 explains the aerodynamic analysis tool and the adaptive mesh refinement technique considered in this

paper. Section 4 presents the solution of two real-world design problems. Section 5 delivers conclusions and futures.

2. Optimization method

2.1. Genetic Algorithms

Even though the Genetic Algorithms (GAs) take more time to converge to optimal design when compared to the traditional deterministic methods, GAs have capabilities to escape from the local optima and to find the global solution. In addition, GAs are based on a fitness function evaluation and no gradients are needed during the optimization process. Beside its applications in a wide range of engineering design problems, GAs have been successfully applied to solve aerodynamic shape optimization problems [6, 7]. Three operators of reproduction, crossover and mutation are utilized in a simple GA. In this paper, the tournament selection without replacement, single point crossover and non uniform mutation are selected. For the constraint handling, the linear penalty method is used such a way that a weighted sum of the individual constraint violation is added to its fitness value if the constraint is not satisfied. Details of GA can be found in Ref. [8].In this research, each generation consists of 20 individuals and the termination criterion is predefined by the number of generation.

2.2. Parameterization for Aerofoil Design

The Bezier curves [14] are utilized to represent the geometry of the airfoil as a linear combination of so called Bezier polynomial. Given a set of $N+1$ control points, the corresponding Bezier curve is defined as

$$\boldsymbol{X}(t) = \sum_{i=0}^{N} B_{i,N}(t)\boldsymbol{R}_i \qquad\qquad B_{i,N} = \binom{n}{i} t^i (1-t)^{n-i} \tag{3}$$

where $t \in [0,1]$ denotes the curve parameter, $B_{i,N}(t)$ are the Bezier polynomials of order N and $\boldsymbol{R}_i$ are the coordinates of the control points. The different smooth curves are created by changing these control points.

The geometries of aerofoil (NACA 0012 and RAE 2822) are represented using 24 control points as shown in Figure 1. To represent the airfoil geometry accurately, the control points are placed close to the zone where the airfoil curve has a bigger curvature. The *y* coordinates of the control points are considered as the design variables while fixing *x* coordinates. Two control points, at the leading edge and trailing edge, have fixed values during the optimization to keep the chord length constant. Also, two other control points near the leading edge are fixed to obtain enough curvature in that zone. In total, twenty design variables are considered for the optimization in Sections 4.1 and 4.2.

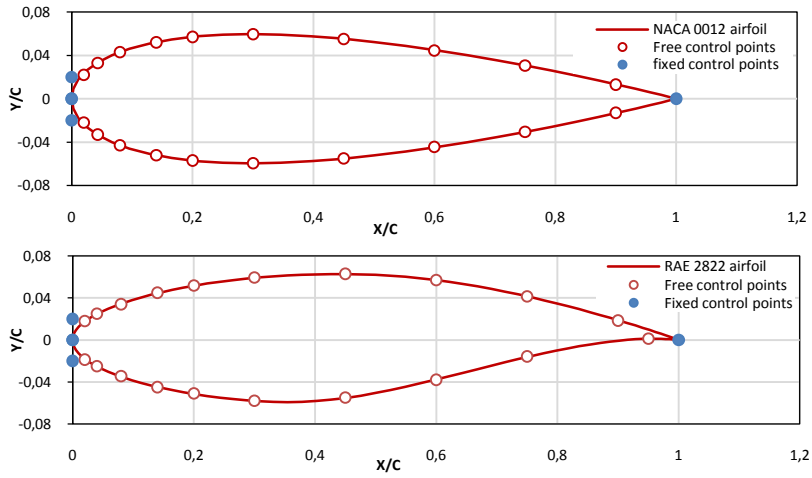

Figure 1: Shape parameterization of NACA 0012 (top) and RAE 2822 (bottom) corresponding free control points and fixed control points

3. Aerodynamic Analysis Tool and Adaptive Remeshing Technique

3.1. Euler solver

In this paper, the PUMI code [21] based on the solution of Euler equations is utilized. Using an Eulerian reference frame, and using conservative variables, the equations can be written as

$$\frac{\partial \boldsymbol{\phi}}{\partial t} + \frac{\partial \mathbf{F}_k}{\partial x_k} = 0 \quad for\ k = 1,2,3 \tag{4}$$

where $\boldsymbol{\phi}$ is the vector of conservative variables and $\mathbf{F}_k$ is the vector of convective flux along the k^{th} direction

$$\boldsymbol{\phi} = \begin{bmatrix} \rho \\ U_1 \\ U_2 \\ U_3 \\ e \end{bmatrix} \quad \mathbf{F}_i = \begin{bmatrix} U_i \\ u_i U_1 + p\delta_{i1} \\ u_i U_1 + p\delta_{i2} \\ u_i U_1 + p\delta_{i3} \\ u_i h \end{bmatrix} \tag{5}$$

where δ_{ij} is the Kronecker delta. The state vector contains the density, momentum ($U_i = \rho u_i$) and total energy (internal plus external) per unit volume of the fluid. Assuming that the fluid behaves like an ideal gas, the expression for the total energy, enthalpy and equation of states are

$$e = \rho\left(c_v T + \frac{u^2}{2}\right) \qquad h = e + p = \rho\left(c_p T + \frac{u^2}{2}\right) \qquad p = \rho RT \qquad R = c_p - c_v \tag{6}$$

After some calculations, the finite element approximation to the equation set (4) is obtained as

$$\int_\Omega N_i \left(N_j \dot{\boldsymbol{\phi}}^j + \frac{\partial \mathbf{F}_k}{\partial x_k}\right) d\Omega = 0 \qquad for\ i = 1, \dots, n_{node} \tag{7}$$

In Eq. (7), there are as many equations as unknowns therefore the system can be solved for the nodal values of the approximate solution by applying proper boundary conditions. The integrals in Eq. (7) are evaluated using a Gauss quadrature. It is assumed that the fluxes inside the elements can be interpolated from their nodal values to increase the efficiency of the algorithm. This is equivalent to use a Lobato quadrature for the fluxes and it does not affect the final results significantly. It is the form of

$$\mathbf{F}_k = N_j \mathbf{F}_k(x^j) = N_j \mathbf{F}_k^j \tag{8}$$

With this assumption, Eq. (7) can be transformed into Eq. (9)

$$\int_\Omega N_i \left(N_j \dot{\boldsymbol{\phi}}^j + \frac{\partial N_j}{\partial x_k}\left(\mathbf{F}_k^j\right)\right) d\Omega = 0 \qquad for\ i = 1, \dots, n_{node} \tag{9}$$

By defining $\mathbf{M}$ as the consistent finite element mass matrix and $\mathbf{r}$ as the residual vector, the final equation set can be written as Eq. (10)

$$\begin{aligned} \dot{\boldsymbol{\phi}}^j &= \mathbf{M^{-1}r} \\ \mathbf{M} &= \int_\Omega N_i N_j d\Omega \\ \mathbf{r} &= \int_\Omega N_i \frac{\partial N_j}{\partial x_k} d\Omega \mathbf{F}_k^j \end{aligned} \tag{10}$$

For time integration, an explicit multi-stage Runge-Kutta scheme is chosen in order to increase the allowable time step.

3.2. Adaptive Remeshing Strategy

For the compressible flow using linear shape functions, two main categories of error indicators are developed by the researchers [4]. The first one is based on the gradient of a flow variable

$$\in_{el}^h = ch|\nabla u| \tag{1}$$

where c is a constant, h is the element size and u is one of the flow variables such as Mach number or density [4]. In the second category, the error indicator can be approximated by a derivative one order higher than the interpolation functions [3, 5]. For the linear elements, the error indicator is shown in Eq. (2)

$$\in_{el}^h = ch^2 \left|\frac{\partial^2 u}{\partial x^2}\right| \tag{2}$$

This paper uses a combination of gradient based and curvature based error indicators [17]. In addition, it is also necessary to use recovery approach due to the zero derivatives of u inside the element and non-continuity functions at the element boundaries.

Once the FEM error is obtained, the elements which need refinement or coarsening can be identified. Then, a mesh refinement strategy should be utilized to coarsen or refine the mesh where the error is less or greater than a desirable value. To do so several methodologies can be introduced including R-method [15, 16], Mesh

enrichment (H refinements) [1] and adaptive remeshing [2, 3]. In this paper, the adaptive remeshing technique is used.

For an efficient adaptive remeshing technique, it is necessary to have a reliable estimation for the new element size as a function of discretization error. In this paper, the error indicator *E* introduced by Löhner [17], is used. *E* can be defined as Eq. (11)

$$\left(E^{\text{old}}\right)_{kl}^{i} = \frac{(D^2)_{kl}^{i}}{(D^1)_{kl}^{i} + (D^0)_{kl}^{i}} \qquad for\ k,l = 1,2,3 \tag{11}$$

where $\left(E^{\text{old}}\right)^{i}$ is the error corresponding to i^{th} node and

$$\begin{aligned} (D^0)_{kl}^{i} &= h^2 c_n \int_{\Omega} \left|N_{,k}^{i}\right|\left|N_{,l}^{j}\right|\left|U_j\right| d\Omega \\ (D^1)_{kl}^{i} &= h^2 \int_{\Omega} \left|N_{,k}^{i}\right|\left|N_{,l}^{j} U_j\right| d\Omega \\ (D^2)_{kl}^{i} &= h^2 \left|\int_{\Omega} N_{,k}^{i} N_{,l}^{j} U_j d\Omega\right| \end{aligned} \tag{12}$$

where c_n is a constant depending on the discretization technique, N^j is the shape function of j^{th} node and U_j is the flow variable of j^{th} node such as Mach number or density. Therefore, the error matrix **E** is obtained as

$$\mathbf{E}^{\text{old}} = \begin{bmatrix} E_{xx}^{old} & E_{xy}^{old} & E_{xz}^{old} \\ E_{yx}^{old} & E_{yy}^{old} & E_{yz}^{old} \\ E_{zx}^{old} & E_{zy}^{old} & E_{zz}^{old} \end{bmatrix} \tag{13}$$

It is assumed that the new element size h^{new} is proportional to old element size h^{old} by a factor called ζ which is defined as

$$\zeta = \frac{h^{\text{new}}}{h^{\text{old}}} \tag{14}$$

The improved error related to the new mesh has the form shown in Eq. (15)

$$(E^{\text{new}})_{kl}^{i} = \frac{\zeta^2\ (D^2)_{kl}^{i}}{\zeta\ (D^1)_{kl}^{i} + (D^0)_{kl}^{i}} \tag{15}$$

Given the desired error indicator value E^{new} for the improved mesh, the reduction factor ζ is given by

$$\zeta_{kl}^{I} = \frac{E^{\text{new}}}{(E^{\text{old}})_{kl}^{I}} \frac{1}{2} \frac{(D^1)_{kl}^{I} + \sqrt{[(D^1)_{kl}^{I}]^2 + 4\ (D^0)_{kl}^{I} \frac{(E^{\text{old}})_{kl}^{I}}{E^{\text{new}}} [(D^1)_{kl}^{I} + (D^0)_{kl}^{I}]}}{[(D^1)_{kl}^{I} + (D^0)_{kl}^{I}]} \tag{16}$$

In 2D case, once ζ_{xx} and ζ_{yy} are obtained for each element, the minimum of these two values is replaced in Eq. (14) to calculate the new element size h^{new}. It is worth noting that in the current methodology only one new element size is prescribed for each element and stretching is not considered. This value is assigned to the corresponding element in a background mesh to generate a new mesh. By predefining the minimum and maximum element size, the computed element size is checked to be in this desirable range. If this condition is not satisfied, the minimum or maximum element size will be assigned.

An automatic grid generator is needed to generate the new mesh using the information obtained from the old mesh. The interpolation technique for the unknown mesh variables from the previous mesh to the new one is implemented at the end of each remeshing level. The most robust one which is implemented here is advancing front technique. In this paper, the minimum element size and desired error, several remeshing levels are predefined to guarantee to have a fine mesh at the final level of remeshing.

3.3. Validation of PUMI and Adaptive remeshing

In this section one numerical example is presented to validate PUMI software and also to illustrate the performance of the adaptive remeshing method. The mesh generation and mesh refinement are carried out using the GiD pre/post processing system implementing advanced front technique.

This example computes a transonic flow over NACA 0012 profile with a freestream Mach number $M_\infty = 0.8$ and angle of attack $\alpha = 1.25^\circ$. Once the analysis starts, PUMI iterates the physical model with predefined time-steps until a predefined density residual is reached (herein 1×10^{-6}). Then, the first refinement level is done. Consecutive refinement levels are carried out every 200 time-steps. In the first step, the computational domain is

discretized by an unstructured mesh consisting of 2,084 nodes and 3,970 elements as shown in Figure 2 a. This mesh conditions will be applied to all the test cases in this paper. Figure 2 b shows the final adaptive mesh consisting of 8,234 nodes and 16,542 elements. It can be seen that the adaptive refinements are particularly applied where the shocks occur on the suction and pressure sides of aerofoil, and the trailing and leading edges. The solution obtained with the adaptive remeshing scheme has been compared with the solution obtained with the uniform mesh shown in Figure 3 consisting of 6,554 nodes and 12,247 elements.

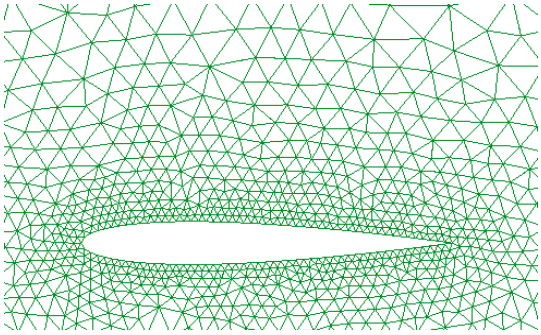

Figure 2 a: Initial (left) mesh around NACA 0012.

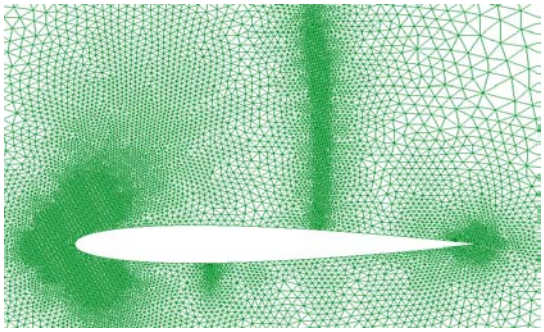

Figure 2 b: Final (right) mesh around NACA 0012.

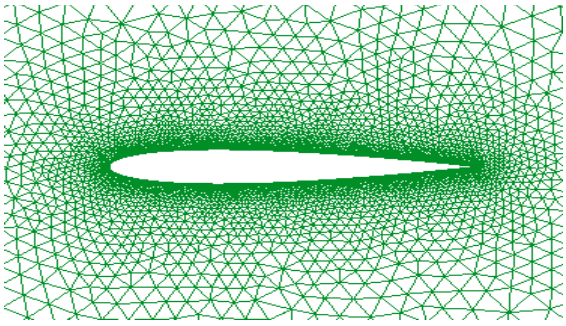

Figure 3: Uniform mesh around NACA 0012.

Figure 4 compares the C_p distributions obtained with the uniform, the adaptive remeshing technique coupled with PUMI and the AGARD solution [18] which is validated by comparing results with the wind tunnel data. It can be seen that numerical results obtained by both uniform and adaptive remeshing techniques are in good agreement with AGARD. Figure 5 shows C_p contour of NACA 0012 obtained by the adaptive final mesh.

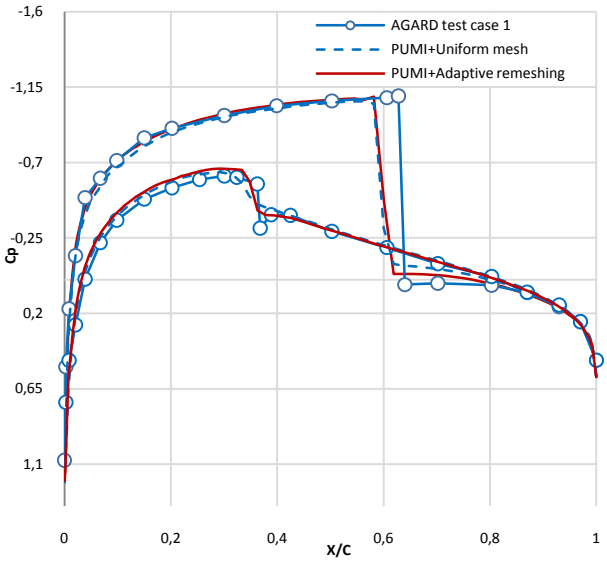

Figure 4: C_p distribution comparison.

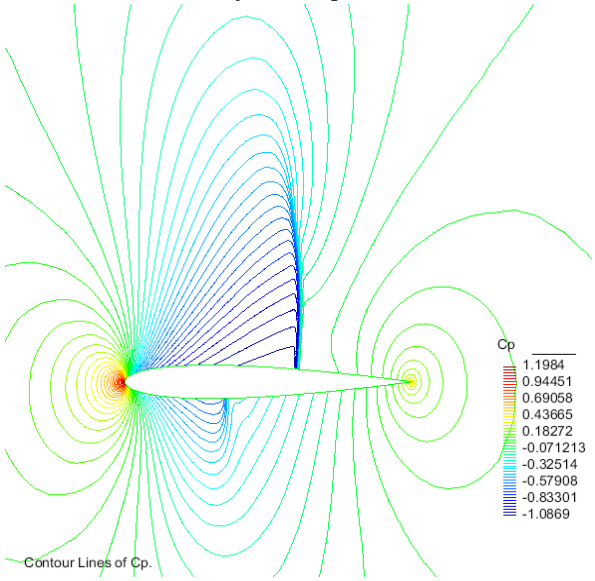

Figure 5: C_p contour of the final mesh around NACA 0012.

4. Real world test cases:

In this section, transonic aerofoil design optimizations for drag minimization and reconstruction design are considered. Based on the concept of single-objective design, the flight conditions of Mach number and angle of attack are treated as constant value with thickness constraint. To demonstrate the benefit of mesh refinement, the results obtained with and without adaptive remeshing are compared. A fine mesh is used for the uniform mesh test cases in such a way that takes a similar computational cost for CFD analysis of adaptive mesh test cases.

4.1. Transonic Aerofoil Design Optimization for Drag minimization

Statement of the problem

The test case considers a single-objective design problem for transonic aerofoil to improve aerodynamic efficiency at the flow conditions $M_\infty = 0.75$ and $\alpha = 3.0^\circ$. The fitness function with thickness constraint is shown in Eq. (17)

$$f = \min\left(\frac{1}{L/D}\right) \quad \text{subject to} \quad \left(\frac{t}{c}\right)_{max} \geq 0.12 \tag{17}$$

where L/D and *t/c* represent the lift to drag ratio and the thickness ratio of the airfoil, respectively.

In other words, the inverse of lift to drag ratio is minimized at specified flight conditions while maintaining the maximum thickness of the baseline design (RAE 2822). For the design variables twenty *y* coordinates with twenty fixed *x* coordinates on the suction and pressure sides of aerofoil are considered, as shown in Section 2.2.

Numerical results

As illustrated in Figure 6, both algorithms coupled to the uniform and adaptive remeshing technique were allowed to run for 50 hours and 150 generations using a single 4 × 2.8 GHz processor. The uniform mesh test case converged to $f = 0.02979$ after 50 hours while this fitness value is already captured by the adaptive remeshing technique after 2.5 hours. In other words, the optimization using adaptive remeshing technique is 95% efficient when compared to the one using the uniform meshing technique. The fitness value resulted from the baseline design and the optimized ones are compared in Table 1. It can be seen that both optimal airfoils obtained by the uniform and adaptive mesh techniques improve aerodynamic efficiency by 47% and 29% respectively.

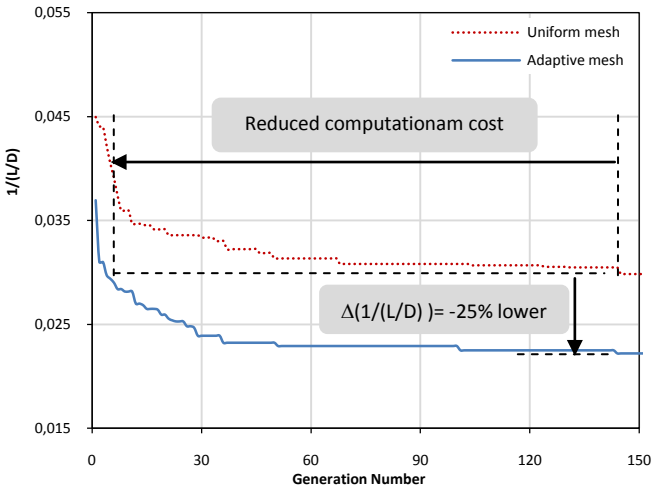

Figure 6: Convergence history for drag minimization.

Table 1: Comparison of fitness function values obtained from baseline RAE 2822, adaptive mesh and uniform mesh test cases.

	Baseline	*Adaptive mesh*	Uniform mesh
$\left(\frac{1}{L/D}\right)$	0.04232	*0.02221 (-47 %)*	0.02979 (-29 %)

The geometries of baseline and optimal airfoils obtained by the uniform and adaptive mesh techniques are compared as shown in Figure 7. Table 2 compares the airfoil characteristics such as the maximum thickness, maximum camber for the baseline design and optimal airfoils from the uniform and adaptive mesh techniques. Both optimal airfoils from the uniform and adaptive mesh techniques have lower camber while maintaining similar thickness ratio when compared to the baseline design.

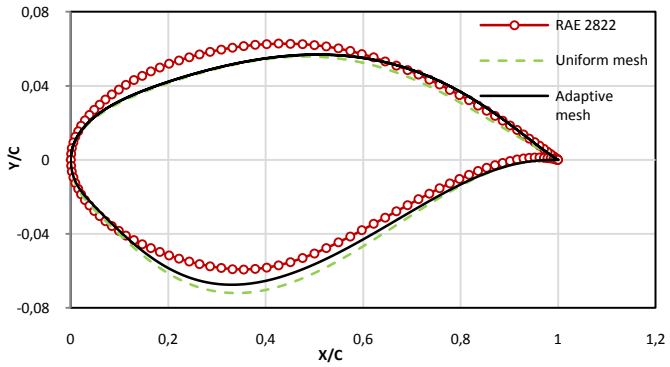

Figure 7: The comparison between the baseline RAE 2822, the adaptive mesh and uniform mesh test case.

Table 2: Airfoil configuration of the baseline RAE 2822 and optimized airfoils using adaptive mesh and uniform mesh

	Baseline	Adaptive mesh	Uniform mesh
t/c_{max}	12.11 % (@ 37.8%)	12.04 % (@ 37.8%)	12.48 % (@ 37.8%)
$camber_{max}$	1.264 % (@ 75.8%)	1.175 % (@ 78.6%)	1.180 % (@ 78.6%)

The Cp distributions obtained by the baseline design, uniform mesh and adaptive mesh techniques are compared as shown in Figure 8. It can be seen that the optimal airfoil obtained by the adaptive meshing has a weaker shockwave when compared to the baseline design and the uniform meshing optimal solution.

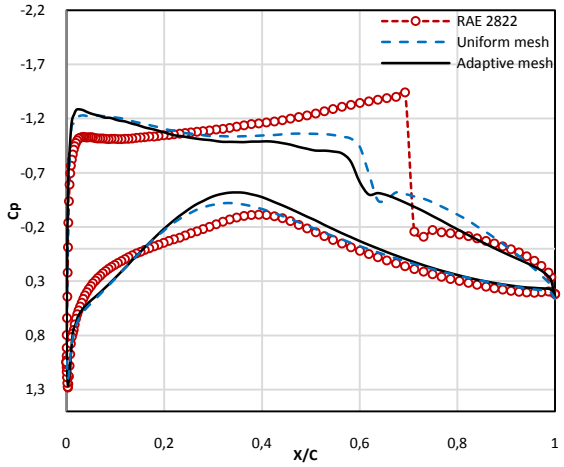

Figure 8: C_p distribution obtained from baseline, adaptive mesh and uniform mesh test cases.

Figure 9 compares Cp contours obtained by the baseline design and the optimal airfoil from the adaptive remeshing optimization. It can be seen that the strong shock wave on the suction side of the baseline design is

getting weaker by optimizing aerofoil geometry especially lower camber (mentioned in Table 2). The drag minimization approach has been successful to lower the strength of shock wave on the suction side of the baseline design.

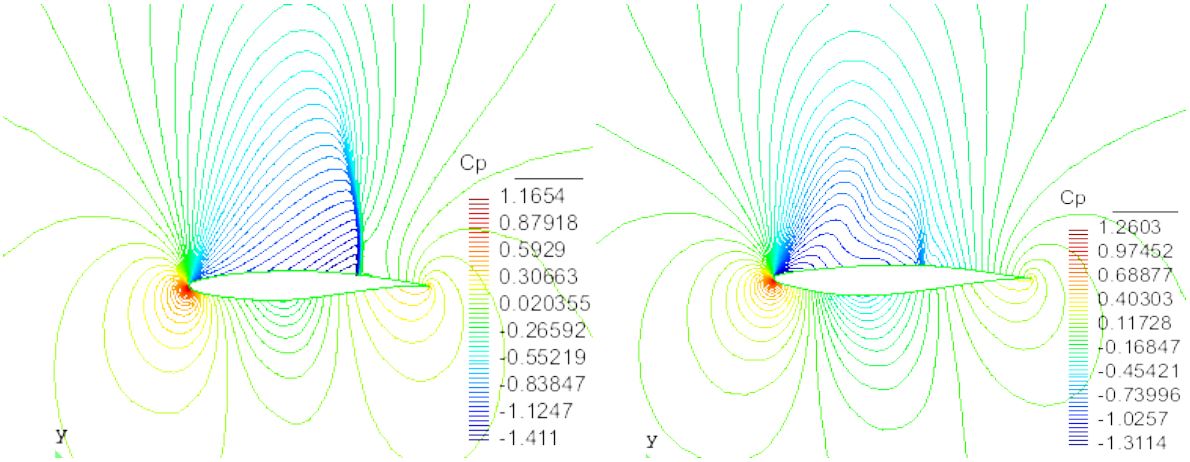

Figure 9: Comparison between C_p contours of RAE 2822 (left) and adaptive mesh test case (right).

4.2. Reconstruction Design Optimization of Transonic Aerofoil

Statement of the problem

This test case considers a single-objective reconstruction design at the flow conditions $M_\infty = 0.75$ and $\alpha = 3.0°$. The main objective is to minimize the pressure error between the target pressure and the candidate. Even though the optimal airfoil obtained by the adaptive remeshing technique (Section 4.1) is selected as a target airfoil, a finer uniform mesh which can compute the same *Cp* distribution of the adaptive remeshing optimal solution is used to make a fair comparison. The fitness function (the least square error of the pressure) is shown in Eq. (18).

$$f = \min\left(\text{Pressure}_{\text{error}}\right) = \min \sum_{i=1}^{N} (Cp - Cp^*)^2 \tag{18}$$

where *N* represents the pressure points (*N* = 200).

Numerical results

As illustrated in Figure 10, both algorithms coupled to the uniform and adaptive remeshing technique were allowed to run for 333 hours and 1,000 generations using a single 4 × 2.8 GHz processor. The uniform mesh test case converged after 566 generations (188 hours) with pressure error of 9.93. The adaptive remeshing technique on the other hand captures this fitness value after 36 generations (12 hours) which is only 7% computational cost of the optimization using the uniform mesh technique. This reflects that the adaptive remeshing technique improves the efficiency of optimization by 93%. Table 3 compares the final pressure errors obtained by the uniform and adaptive mesh techniques. It is shown that the adaptive remeshing test case produces 38% lower pressure error than the uniform mesh test case.

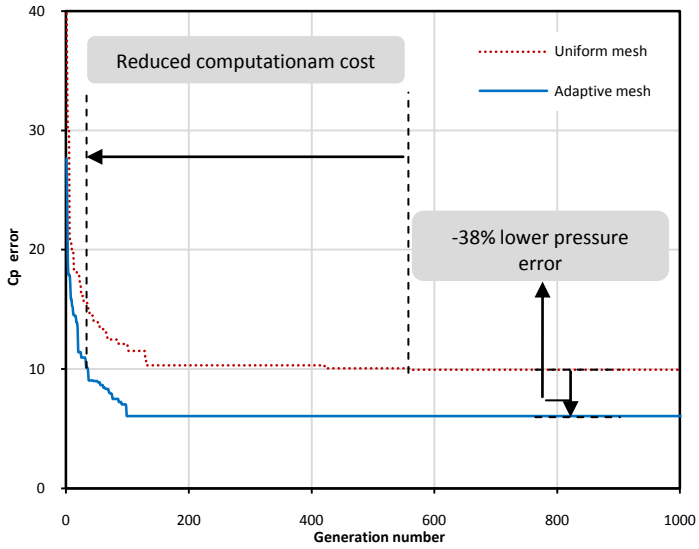

Figure 10: Convergence history of reconstruction design of uniform and adaptive mesh test cases

Table 3: Comparison of fitness function values obtained from adaptive mesh and uniform mesh test cases.

	Adaptive mesh	Uniform mesh
Pressure error	*6.08 (- 38%)*	9.93

Figures 11 and 12 compare the airfoil geometries and pressure distributions obtained by the target and both mesh techniques. It can be seen that the optimal aerofoil obtained by the adaptive mesh technique has a better agreement to the target when compared to the solution from the uniform mesh test case.

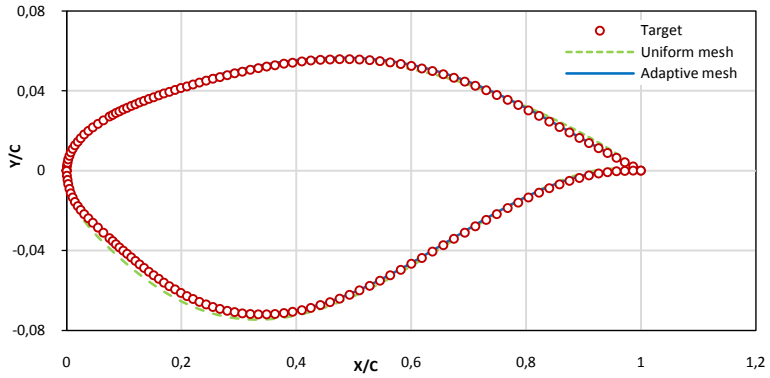

Figure 11: Comparison between target , uniform mesh test case and adaptive mesh test case airfoils

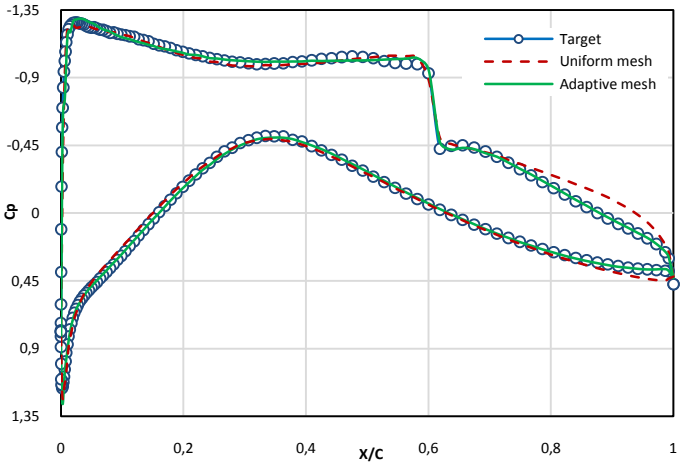

Figure 12: Comparison between target , uniform mesh test case and adaptive mesh test case Cp distributions

7. Conclusion

This research work shows the results obtained with an adaptive remeshing scheme coupled with a GA and a CFD analysis tool when solving two practical transonic airfoil design optimization problems. Numerical results obtained from both drag minimization and reconstruction design optimization problems show that the optimization coupled with the adaptive remeshing technique converges 95% faster with 38% results accuracy improvement when compared to the one with the uniform mesh. Future studies will focus on implementation of the adaptive remeshing technique in a multi-objective/point design optimization under considering uncertain design parameters (robust/uncertainty).

8. Acknowledgement

The authors greatly acknowledge Jordi Pons for helpful discussions and suggestions, Enrique Ortega for providing CFD solver and also GiD group in CIMNE.

Reference:

1. Löhner R. *An Adaptive Finite Element Scheme for Transient Problems in CFD,* Comp. Meth. Appl. Mech. Eng. 61, 323–338 (1987).
2. Löhner R., *Adaptive Remeshing for Transient Problems,* Comp. Meth. Appl. Mech. Eng. 75, 195–214 (1989).
3. Peraire J., Vahdati M., Morgan K. and Zienkiewicz O.C., *Adaptive Remeshing for Compressible Flow Computations,* J. Comp. Phys. 72, 449–466 (1987).
4. Zienkiewicz O.C., Wu J., *Automatic directional refinement in adaptive analysis of compressible flows,* International Journal for Numerical Methods in Engineering; 37:2189-2210 (1994).
5. Nithiarasu P., and Zienkiewicz O.C., *Adaptive mesh generation for fluid mechanics problems,* Internat. J. for Num. Meth. in Eng., 47:629-662 (2000).
6. Quagliarella D. and Cioppa A. D., *Genetic Algorithms applied to the Aerodynamic Design of Transonic Airfoils,* AIAA-94-1896-CP (1994).
7. Yamamoto K. and Inoue O., *Applications of Genetic Algorithm to Aerodynamic Shape Optimization,* AIAA Paper 95-1650-CP, A collection of technical papers, 12th AIAA Computational Fluid Dynamics Conference, CP956, San Diego, CA, 43-51 (1995).
8. Goldberg D.E., *Genetic Algorithm in Search, Optimization and Machine Learning,* Massachusetts, Addison-Wesley (1989).
9. Flores R., Ortega E. and Oñate E., *PUMI: an explicit 3D unstructured finite element solver for the Euler equations*, Publication CIMNE PI 326 (2008).
10. Obayashi S. and Oyama A., *Three- Dimensional Aerodynamic Optimization with Genetic Algorithms,* Proceedings of the Third ECCOMAS Computational Fluid Dynamics Conference, John Wiley & Sons, Ltd, Chichester, U.K., 420-424 (1996).
11. Holst T. L. and Pulliam T. H., *Aerodynamic Shape Optimization Using a Real- Number-Encoded Genetic Algorithm,* AIAA Paper 2001-2473 (2001).
12. Volpe G. and Melnik R. E., *The design of transonic airfoils by a wellposed inverse method*. International Journal for Numerical Methods in Engineering, 22, 341-361 (1984).
13. Periaux J., D.S. Lee, Gonzalez L.F. and Srinivas K., *Fast Reconstruction of Aerodynamic Shapes using Evolutionary Algorithms and Virtual Nash Strategies in a CFD Design Environment,* Journal of Computational and Applied Mathematics, 232, 61-67 (2009).
14. Faux I.D. and Pratt M.J., *Computational Geometry for Design and Manufacture*, Ellis Horwood Limited (1987).
15. Palmerio B. and Dervieux A., *Application of a FEM Moving Node Adaptive Method to Accurate Shock Capturing,* Proc. First Int. Conf. on Numerical Grid Generation in CFD, Landshut, W. Germany (1986).
16. Jacquotte O. P. and Cabello J., *Three-Dimensional Grid Generation Method Based on a Variational Principle,* Rech. Aerosp., 1990-4, 8–19 (1990).
17. Löhner R., *Mesh adaptation in fluid mechanics,* Eng. Fracture Mech. 50(5/6), 819 (1995).
18. Pulliam TH., Barton JT., *Euler computations of AGARD Working Group 07 Airfoil Test Cases.* AIAA 23rd Aerospace Summer Meeting, Reno, NE, AIAA Paper 85-0018 (1985).